Structure and stability of recombinant bovine odorant-binding protein: II. Unfolding of the monomeric forms

Olga V Stepanenko, Denis O Roginskii, Olesya V Stepanenko, Irina M Kuznetsova, Vladimir N Uversky, Konstantin K Turoverov

In a family of monomeric odorant-binding proteins (OBPs), bovine OBP (bOBP), that lacks conserved disulfide bond found in other OBPs, occupies unique niche because of its ability to form domain-swapped dimers. In this study, we analyzed conformational stabilities of the recombinant bOBP and its monomeric variants, the bOBP-Gly121+ mutant containing an additional glycine residue after the residue 121 of the bOBP, and the GCC-bOBP mutant obtained from the bOBP-Gly121+ form by introduction of the Trp64Cys/His155Cys double mutation to restore the canonical disulfide bond. We also analyzed the effect of the natural ligand binding on the conformational stabilities of these bOBP variants. Our data are consistent with the conclusion that the unfolding-refolding pathways of the recombinant bOBP and its mutant monomeric forms bOBP-Gly121+ and GCC-bOBP are similar and do not depend on the oligomeric status of the protein. This clearly shows that the information on the unfolding-refolding mechanism is encoded in the structure of the bOBP monomers. However, the process of the bOBP unfolding is significantly complicated by the formation of the domain-swapped dimer, and the rates of the unfolding-refolding reactions essentially depend on the conditions in which the protein is located.

PeerJ PrePrints | https://dx.doi.org/10.7287/peerj.preprints.1452v1 | CC-BY 4.0 Open Access | rec: 27 Oct 2015, publ: 27 Oct 2015

Structure and Stability of Recombinant Bovine Odorant-Binding Protein: II. Unfolding of the Monomeric Forms

Olga V. Stepanenko,[1] Denis O. Roginskii,[1] Olesya V. Stepanenko,[1] Irina M. Kuznetsova,[1] Vladimir N. Uversky,[1,2,*] and Konstantin K. Turoverov[1,3,*]

[1]*Laboratory of structural dynamics, stability and folding of proteins, Institute of Cytology, Russian Academy of Sciences, St. Petersburg, Russia;*

[2]*Department of Molecular Medicine and USF Health Byrd Alzheimer's Research Institute, Morsani College of Medicine, University of South Florida, Tampa, FL, USA;*

[3]*Peter the Great St. Petersburg Polytechnic University, St. Petersburg, Russia*

***To whom correspondence should be addressed**: VNU, Department of Molecular Medicine, University of South Florida, 12901 Bruce B. Downs Blvd. MDC07, Tampa, Florida 33612, USA, E-mail: vuversky@health.usf.edu; KKT, Institute of Cytology, Russian Academy of Sciences, Tikhoretsky Av., 4, St. Petersburg 194064, Russia, E-mail: kkt@incras.ru

Running title: Unfolding of the monomeric bOBP variants

ABSTRACT

In a family of monomeric odorant-binding proteins (OBPs), bovine OBP (bOBP), that lacks conserved disulfide bond found in other OBPs, occupies unique niche because of its ability to form domain-swapped dimers. In this study, we analyzed conformational stabilities of the recombinant bOBP and its monomeric variants, the bOBP-Gly121+ mutant containing an additional glycine residue after the residue 121 of the bOBP, and the GCC-bOBP mutant obtained from the bOBP-Gly121+ form by introduction of the Trp64Cys/His155Cys double mutation to restore the canonical disulfide bond. We also analyzed the effect of the natural ligand binding on the conformational stabilities of these bOBP variants. Our data are consistent with the conclusion that the unfolding-refolding pathways of the recombinant bOBP and its mutant monomeric forms bOBP-Gly121+ and GCC-bOBP are similar and do not depend on the oligomeric status of the protein. This clearly shows that the information on the unfolding-refolding mechanism is encoded in the structure of the bOBP monomers. However, the process of the bOBP unfolding is significantly complicated by the formation of the domain-swapped dimer, and the rates of the unfolding-refolding reactions essentially depend on the conditions in which the protein is located.

Key words: odorant-binding protein; domain swapping; disulfide bond; unfolding-refolding reaction; ligand binding; conformational stability

INTRODUCTION

Odorant binding proteins (OBPs) are important components of olfactory apparatus in vertebrates where they play a specific role in olfaction by interacting directly with odorants (Xu et al. 2005). OBPs constitute a class of small extracellular proteins in the chemosensory systems of most terrestrial species ranging from drosophila to human. In mammals, OBPs are found at high concentrations (~10 mM) in nasal mucosa of cow (Bignetti et al. 1985; Pelosi et al. 1982), rat (Pevsner et al. 1985), rabbit (Dal Monte et al. 1991), pig (Dal Monte et al. 1991), dog (D'Auria et al. 2006), and humans (Briand et al. 2002). Although they bind different kinds of small and hydrophobic odorant molecules (typically with the affinities in the micromolar range, their inability to discriminate different chemical classes of these molecules suggests that OBPs cannot serve as olfactory receptors (Boudjelal et al. 1996). The precise biological functions of mammalian OBPs are not known as of yet, but it was hypothesized that these proteins can be involved in transport of hydrophobic odorants across the aqueous mucus layer to access the olfactory receptors, or might be involved in the termination of the olfactory signal by removing odorants from the receptors after their stimulation (Bignetti et al. 1987; Pevsner & Snyder 1990).

OBPs constitute a sub-class of lipocalins, which are small extracellular proteins found in gram negative bacteria, plants, invertebrates, and vertebrates. Although lipocalins are known to share limited regions of sequence homology, they do have a common tertiary structure architecture (Flower et al. 2000; Grzyb et al. 2006). The characteristic structural signature of the lipocalin family is a β-barrel composed by a 9-stranded anti-parallel β-sheet with an α-helical segment at the C-terminus (Flower et al. 2000). The internal cavity of the lipocalin β-barrel is the binding site that can interact with the odorant molecules

belonging to different chemical classes (Vincent et al. 2000). Bovine OBP (bOBP) was the first OBP for which crystal structure was solved, and the analysis of this structure revealed that bOBP exists as a domain-swapped dimer (Bianchet et al. 1996; Tegoni et al. 1996). This was in contrast to structures of other lipocalins, including the porcine OBP (pOBP) (Spinelli et al. 1998), which are monomeric proteins. The ability of bOBP to form domain-swapped dimers was explained by the absence of a glycine residue at the hinge region linking the β-barrel to the α–helix, and by the lack of the disulfide bridge which is present in all lipocalin sequences identified so far (Ramoni et al. 2002).

This work is dedicated to the analysis of the peculiarities of the GdnHCl-induced unfolding – refolding reactions of the recombinant bOBP and its monomeric mutants, bOBP-Gly121+ and bOBP-Gly121+/W64C/H155C (GCC-bOBP). It continues a series of articles dedicated to the analysis of the effect of the environmental feature (including the presence of crowding agents) on structural properties and conformational stability of bOBP. The mutant protein bOBP-Gly121+ contains an extra glycine residue introduced after the bOBP residue 121. This substitution was shown to promote monomerization of the bOBP (Stephanenko et al. 2015) likely via increasing the mobility of the loop connecting α-helix and 8th β-strand of the β-barrel. Substitutions of the residues Trp64 and His156 to cysteines in bOBP-Gly121+ generate a mutant form GCC-bOBP, which is expected to have stable monomeric structure due to the restoration of the disulfide bond typically seeing in other OBPs (Ramoni et al. 2008). We also investigated the role of the natural ligand in the stabilization of protein structure and looked at how the ligand binding affected the folding-unfolding reaction of these proteins.

MATHERIAL AND METHODS

Materials

GdnHCl (Nacalai Tesque, Japan), 1-octen-3-ol (OCT; Sigma-Aldrich, USA) and ANS (ammonium salt of 8-anilinonaphtalene-1-sulfonic acid; Fluka, Switzerland) were used without further purification. The protein concentration was 0.1 – 0.2 mg/ml. The OCT concentration was 10 mM. The experiments were performed in 20 mM Na-phosphate-buffered solution at pH 7.8.

Gene expression and protein purification

The plasmids pT7-7-bOBP which encodes bOBP and its mutant forms with a poly-histidine tag were used to transform *Escherichia coli* BL21(DE3) host (Invitrogen) (Stepanenko et al. 2014c). The protein expression was induced by incubating the cells with 0.3 mM of isopropyl-beta-D-1-thiogalactopyranoside (IPTG; Fluka, Switzerland) for 24 h at 37 °C. The recombinant protein was purified with Ni+-agarose packed in HisGraviTrap columns (GE Healthcare, Sweden). The protein purity was determined through SDS-PAGE in 15% polyacrylamide gel (Laemmli 1970).

Fluorescence spectroscopy

Fluorescence experiments were performed using a Cary Eclipse spectrofluorometer (Varian, Australia) with microcells FLR (10 x 10 mm; Varian, Australia). Fluorescence lifetime were measured using a “home built” spectrofluorometer with a nanosecond impulse (Stepanenko et al. 2014a; Stepanenko et al. 2012; Turoverov et al. 1998) as well as micro-cells (101.016-QS 5 x 5 mm; Hellma, Germany). Tryptophan fluorescence in the protein was excited at the long-wave

absorption spectrum edge (λ_{ex} = 297 nm), wherein the tyrosine residue contribution to the bulk protein fluorescence is negligible (Stepanenko et al. 2015). The fluorescence spectra position and form were characterized using the parameter $A = I_{320}/I_{365}$, wherein I_{320} and I_{365} are the fluorescence intensities at the emission wavelengths 320 and 365 nm, respectively (Turoverov & Kuznetsova 2003). The values for parameter *A* and the fluorescence spectrum were corrected for instrument sensitivity. The tryptophan fluorescence anisotropy was calculated using the equation: $r = (I_V^V - GI_H^V)/(I_V^V + 2GI_H^V)$, wherein I_V^V and I_H^V are the vertical and horizontal fluorescence intensity components upon excitement by vertically polarized light. *G* is the relationship between the fluorescence intensity vertical and horizontal components upon excitement by horizontally polarized light ($G = I_V^H / I_H^H$), λ_{em} = 365 nm (Turoverov et al. 1998). The fluorescence intensity for the fluorescent dye ANS was recorded at λ_{em} = 480 nm (λ_{ex} = 365 nm).

GdnHCl-induced unfolding

Protein unfolding was initiated by manually mixing the protein solution (40 μL) with a buffer solution (510 μL) that included the necessary GdnHCl concentration in the absence or presence of a natural ligand, 1-Octen-3-ol (OCT). The GdnHCl concentration was determined by the refraction coefficient using an Abbe refractometer (LOMO, Russia; (Pace 1986)). The dependences of different fluorescent characteristics of the studied proteins on GdnHCl were recorded following protein incubation in a solution with the appropriate denaturant concentration at 4ºC for different times (see in the text). The protein refolding was initiated by diluting the pre-denatured protein (in 3.0 M GdnHCl, 40 μL) with the buffer or denaturant solutions at various

concentrations (510 µL). The spectrofluorimeter was equipped with a thermostat that holds the temperature constant at 23°C.

Circular dichroism measurements

The CD spectra were generated using a Jasco-810 spectropolarimeter (Jasco, Japan). Far-UV CD spectra were recorded in a 1-mm path length cell from 260 nm to 190 nm with a 0.1 nm step size. For the spectra, we generated 3 scans on average. The CD spectra for the appropriate buffer solution were recorded and subtracted from the protein spectra.

Gel filtration experiments

We performed gel filtration experiments for recombinant bOBPwt and its mutant forms in a buffered solution and with addition of GdnHCl using a Superdex-75 PC 3.2/30 column (GE Healthcare, Sweden) and an AKTApurifier system (GE Healthcare, Sweden). The column was equilibrated with the buffered solution or GdnHCl at the desired concentration, and 10 µl of the protein solution prepared under the same conditions was loaded on the pre-equilibrated column. The change in hydrodynamic dimensions for the studied proteins was evaluated as a change in the protein elution volume. Multiple proteins with known molecular masses (aprotinin (6.5 kDa), ribonuclease (13.7 kDa), carbonic anhydrase (29 kDa), ovalbumin (43 kDa) and conalbumin (75 kDa), which are chromatography standards from GE Healthcare) were used to generate the calibration curve.

RESULTS AND DISCUSSION

Structural features of the monomeric and dimeric bOBPs

Figure 1 compares structural features of the natural bOBP and its monomeric mutant GCC-bOBP. Structures shown in Figures 1A and 1B indicate that the domain swapping has been reverted in monomeric GCC-bOBP. Furthermore, Figure 1C represents the results of the multiple structural alignment of the one of the monomers of the natural dimeric bOBP (blue structure), monomeric mutant GCC-bOBP (red structure), and naturally monomeric pOBP (green structure) and clearly shows that the monomeric GCC-bOBP has the overall fold almost identical to that of the pOBP. Next, we analyzed how introduced mutations affected the structural flexibility of bOBP utilizing the power of the FlexPred tool that rapidly predicts absolute per-residue fluctuations from a three-dimensional structure of a query protein (Jamroz et al. 2012). Results of this analysis are shown in Figure 1D which clearly indicates that the chains of the bOBP dimer, chains of the naturally monomeric pOBP and the monomeric mutant GCC-bOBP are all characterized by very similar structural flexibility. We also compared these structure-based flexibility results with the bOBP propensity for intrinsic disorder evaluated by PONDR® VSL2B, which is one of the more accurate stand-alone disorder predictors (Fan & Kurgan 2014; Peng et al. 2005; Peng & Kurgan 2012). Figure 1D clearly shows that there is generally a very good agreement between the structural flexibility calculated from the protein crystal structure and the propensity of a protein for intrinsic disorder.

Equilibrium unfolding of the recombinant bOBP in the presence of natural ligand

Previously we have shown that the recombinant bOBP, unlike the natural bOBP extracted

177 from the tissues, represents a mixture of monomeric and dimeric forms suggesting that this
178 protein exists in a stable native-like state with a reduced dimerization capability (Stepanenko et
179 al. 2014c) (Table 1, Figure 2). It has been suggested that the recombinant form of bOBP is
180 characterized by the disturbed package of the α-helical region and some β-strands, which
181 prevents the formation of a native domain-swapped dimer (Stepanenko et al. 2014c). It is likely
182 that the dimer formation via the domain exchange mechanism is a rather complex process that
183 requires specific organization of the secondary and tertiary structure within the monomers.
184 Curiously, recombinant bOBP can form the compact dimeric state under the mild denaturing
185 conditions, namely, in the presence of 1.5 M guanidine hydrochloride (GdnHCl) (Stepanenko et
186 al. 2014c). This process requires bOBP restructuring and is accompanied by the formation of a
187 stable, more compact, intermediate state that is maximally populated at 0.5 M GdnHCl. The
188 increase of the GdnHCl concentration above 1.5 M induces cooperative unfolding of the
189 recombinant bOBP which is completed by ~3M GdnHCl (Stepanenko et al. 2014c). The half-
190 transition point of this unfolding process at > 2 M GdnHCl indicates high conformational
191 stability of the recombinant bOBP (Stepanenko et al. 2014c), which is comparable with that of
192 the native (isolated from tissue) bOBP (Mazzini et al. 2002) and pOBP (Staiano et al. 2007;
193 Stepanenko et al. 2008) and is inherent to β-rich proteins (Stepanenko et al. 2012; Stepanenko et
194 al. 2013; Stepanenko et al. 2014b). We have also established that the unfolding of recombinant
195 protein is a completely reversible process, whereas the preceding process of the dimerization of
196 recombinant bOBP is the irreversible event (Stepanenko et al. 2014c).

197 To understand how interaction of the recombinant bOBP with its natural ligand, 1-Octen-3-
198 ol (OCT) affects this protein, we investigated structural properties and conformational stability
199 of the recombinant bOBP in the presence and absence of OCT. The formation of the protein-

ligand complex does not affect the oligomeric status of the protein, since according to the gel filtration analysis the protein in the bOBP/OCT complex continue to exist as a mixture of monomeric and dimeric molecules. However, both monomeric and dimeric forms of the protein become more compact as a result of the OCT binding (Table 2, Figure 3). The GdnHCl-induced unfolding of the bOBP/OCT complex is a rather slow process, since the equilibrium unfolding curves are achieved after incubation of the bOBP/OCT in the presence of different concentrations of the denaturing agent for more than 24 hours. However, the established equilibrium was not affected by further incubation for up to 5 days (Figure 4).

Figure 4 shows that the complexity of the bOBP/OCT unfolding is clearly illustrated by the complex shapes of the equilibrium dependencies of various characteristics of this complex on GdnHCl concentration. This suggests the accumulation of several intermediate states, which are similar to partially folded species found during the equilibrium unfolding of the recombinant bOBP in the absence of OCT. However, compared to the bOBP alone, in the case of the unfolding of bOBP/OCT complex, the accumulation of these intermediate states takes place at higher denaturant concentrations. In fact, a more compact intermediate state of the bOBP/OCT complex is formed in the concentration range of 0.26 - 1.0 M GdnHCl, whereas the transition of the bOBP/OCT complex to the dimeric state occurs only at 2.0 M GdnHCl (Figure 3). Increasing the GdnHCl concentration over 2.0 M leads to the cooperative unfolding of the bOBP/OCT complex. In comparison with the unfolding of the recombinant bOBP alone, the unfolding of the bOBP/OCT complex occurs in a narrow concentration range, and higher denaturant concentrations are required for complete unfolding of this complex. All these data indicate that formation of the bOBP/OCT complex leads to the substantial stabilization of the protein, but does not affect its unfolding mechanism.

To better understand the GdnHCl-induced unfolding of the bOBP/OCT complex, we analyzed the dependence of the 8-anilinonaphthalene-1-sulfonic acid (ANS, also called 1-anilino-8-naphthalenesulfonate), fluorescence on the denaturant concentration. This hydrophobic fluorescent probe is frequently used for the analysis of the presence of solvent-exposed hydrophobic patches in a protein (Stryer 1965) and for the detection of accumulation of partially folded intermediates during equilibrium and kinetic protein unfolding-refolding processes due the ability of ANS to bind to such solvent-exposed hydrophobic patches (which are commonly found in partially folded proteins) and due to the fact that this interaction can be easily detected by the significant increase in the ANS fluorescence intensity and a characteristic blue-shift of its fluorescence maximum (Semisotnov et al. 1991). The shape of the unfolding curve monitored by the GdnHCl-induced changes in the fluorescence intensity of ANS added to the bOBP/OCT was remarkably different from the unfolding curve measured for the recombinant bOBP alone. We observe a smooth continuous decrease in the ANS fluorescence intensity at moderate GdnHCl concentrations, with the ANS fluorescence intensity reaching zero at the denaturant concentrations leading to the formation of the compact dimeric form of bOBP (Figure 4).

These observations suggest that ANS interacts with bOBP at sites close to and/or overlapping with the ligand binding sites. Therefore, the formation of the bOBP/OCT complex prevents ANS binding. Earlier analysis of the dimeric bOBP structure revealed the presence of an additional ligand binding site at the interface between the monomeric subunits (Bianchet et al. 1996; Ikematsu et al. 2005; Pevsner et al. 1985). However, this inter-subunit binding site was shown to be noticeably weaker than the major ligand binding site located within the β-barrel (Bianchet et al. 1996; Ikematsu et al. 2005; Pevsner et al. 1985). Our data agree with the presence of an additional ligand binding site in a protein. At the formation of the dimeric

246 bOBP/OCT complex with the native-like compactness at 2.0 M GdnHCl, this additional site is
247 occupied by the ligand, also preventing its interaction with ANS.

248 Moderate ANS fluorescence is detected in solutions containing less than 2 M GdnHCl; i.e.,
249 under conditions where the bOBP/OCT complex exists as a mixture of monomeric and dimeric
250 molecules, which are different from the native dimeric form of the bOBP. Under these
251 conditions, ANS fluorescence intensity in the presence of the bOBP/OCT complex is noticeably
252 lower than the ANS fluorescence recorded for the bOBP alone. These observations suggest that
253 under these conditions the additional ligand binding site of the dimeric bOBP/OCT complex is
254 occupies by ANS, whereas the inner cavity of the barrel is engaged in the ligand binding. It is
255 likely that the inability of the natural ligand to interact with the additional weak ligand binding
256 site located between the monomeric subunits can be due to the structural difference of this site in
257 the native dimeric bOBP and in a protein in the original native-like state or an intermediate
258 compact state.

259 Analysis of the bOBP/OCT refolding from the completely unfolded state revealed that the
260 dependencies of various structural characteristics of the bOBP/OCT on GdnHCl concentrations
261 depend on the incubation time of this complex in the presence of the denaturant (see Figure 4). In
262 fact, during the refolding process, equilibrium values of the analyzed structural characteristics of
263 the bOBP/OCT complex are reached after the incubation of this complex in the presence of the
264 desired GdnHCl concentration for 72 hrs. No subsequent changes were detected when protein
265 was incubated for 30 days. This analysis revealed the presence of noticeable hysteresis between
266 the curves describing the equilibrium unfolding and refolding of the bOBP/OCT complex in a
267 wide range of the GdnHCl concentrations. In fact, the equilibrium unfolding and refolding
268 curves coincide only in the vicinity of 2.0 M GdnHCl, where, according to the gel-filtration

analysis, the native dimeric state of the bOBP/OCT complex is formed, whereas within the region corresponding to the transition from the native dimeric form to the completely unfolded state of the bOBP/OCT complex, equilibrium curves describing unfolding and refolding of this complex do not coincide.

The equilibrium refolding curve describing transition from the unfolded to the compact dimeric state of the bOBP/OCT complex is shifted toward the lower GdnHCl concentrations in comparison with the equilibrium unfolding curve (Figure 4). However, in comparison with the unfolding of the bOBP alone, this equilibrium refolding curve of the bOBP/OCT complex is still shifted toward higher GdnHCl concentrations. These data suggest that at the same denaturant concentrations, the fractions of native bOBP formed during the refolding from the completely unfolded state are significantly lower than the fraction of native protein remaining within the region of the bOBP/OCT unfolding. However, once formed, the native protein gains the ability to bind ligand. This hypothesis is supported by the results of the gel-filtration analysis (Figure 3). For example, the elution profiles registered during the unfolding and refolding of the bOBP/OCT complex at 2.5 M GdnHCl show that under these conditions, more native protein is present during the bOBP/OCT unfolding, whereas unfolded species prevail during the refolding of this complex. Therefore, the effective rates of the formation of various bOBP conformers are significantly different during the unfolding and refolding processes and noticeably depend on the denaturant concentration.

It is likely that the same reasons define the irreversibility of the unfolding of the bOBP/OCT complex at low GdnHCl concentrations. Under these conditions, the rate of the formation of the monomeric bOBP/OCT complex is significantly higher than the rate of the dimeric bOBP/OCT formation. As a result, refolding of the bOBP/OCT complex at the low

GdnHCl concentrations results in the preferential formation of monomeric bOBP/OCT species, whereas under the identical conditions, the unfolding reaction mixture contains roughly equimolar quantities of the bOBP/OCT monomers and dimmers (Figures 3 and 4).

Equilibrium unfolding of the monomeric bOBP-Gly121+

Already at relatively low GdnHCl concentrations, the monomeric bOBP-Gly121+ is converted to the compact partially folded state with structural characteristics resembling those of the partially folded species accumulated during the equilibrium unfolding of the recombinant bOBP (see Figures 5-6 and Table 2). This compact intermediate is able to bind ANS and exists in a wide range of the GdnHCl concentrations (up to about 1.3 M GdnHCl). Subsequent increase in the denaturant concentration promotes transition to a more loose form, which, at the further increase of the GdnHCl concentration, is converted to the completely unfolded state. This GdnHCl-induced unfolding of the bOBP-Gly121+ is a completely reversible process as evidenced by the coincidence of the equilibrium characteristics of the protein measured at the processes of the bOBP-Gly121+ unfolding and refolding.

The formation of the bOBP-Gly121+/OCT complex results in a noticeable stabilization of this protein. This is evidenced by the increase in the cooperativity of the unfolding transition, which is also shifted toward higher GdnHCl concentrations. However, the formation of a complex between the bOBP-Gly121+ and OCT does not affect the unfolding mechanism of this protein.

GdnHCl-induced unfolding of the monomeric GCC-bOBP

Analysis of the peculiarities of the equilibrium unfolding and refolding processes monitored by the GdnHCl-induced changes in various structural characteristics of the monomeric GCC-bOBP suggests that the unfolding of this protein is a completely reversible process accompanied by the formation of partially folded intermediates similar to those observed during the equilibrium unfolding of the recombinant bOBP and its monomeric bOBP-Gly121+ form (see Figures 7-8 and Table 2). However, although qualitatively unfolded processes of these three proteins are similar, there are some noticeable differences. For example, in comparison with the recombinant bOBP and bOBP-Gly121+ unfolding, a compact intermediate with high ANS affinity is formed at higher denaturant concentrations during the GCC-bOBP unfolding (at 1.0 M GdnHCl). This illustrates higher conformational stability of the disulfide-stabilized GCC-bOBP compared to the recombinant bOBP and its monomeric form bOBP-Gly121+.

GCC-bOBP is further stabilized due to the GCC-bOBP/OCT complex formation. Refolding curves detected by changes in different structural characteristics of this complex and registered after the incubation of the corresponding solutions for one hour coincide with the transition curves describing the equilibrium unfolding of GCC-bOBP, and subsequent incubation of these same solutions for 72 hrs leads to the detectable shift of the transition curves. As a result, equilibrium unfolding and refolding transitions of the GCC-bOBP/OCT complex coincide suggesting that the unfolding of this protein is a completely reversible process. However, GCC-bOBP becomes able to bind ligand only after the formation of correct native structure stabilized by the disulfide bond. Earlier similar effects were described for other ligand-binding protein, such as the D-glucose/D-galactose-binding protein (GGBP) from *E. coli* (Stepanenko et al. 2011a; Stepanenko et al. 2009; Stepanenko et al. 2011b). In fact, our analysis of the peculiarities of the GGBP unfolding revealed that ligand binding might constitute a rate-limiting stage of the

337 protein unfolding-refolding process. This phenomenon can be understood considering the fact
338 that the formation of the protein-ligand complex depends on the appearance of the matching
339 configurations between the ligand and the active site of a fully formed native protein
340 (Stepanenko et al. 2011a; Stepanenko et al. 2009; Stepanenko et al. 2011b).

341 Our current analysis revealed that the unfolding of the monomeric complexes bOBP-
342 Gly121+/OCT and GCC-bOBP/OCT is not accompanied by the ANS fluorescence enhancement
343 in the whole range of GdnHCl concentrations (see Figures 6 and 8). These observations support
344 the hypothesis on the existence of the additional ligand-binding site in the dimeric bOBP.

345 Figure 9 shows that the equilibrium unfolding transition recorded for the recombinant
346 bOBP coincides with that of its monomeric bOBP-Gly121+ form. On the other hand, unfolding
347 transition of the monomeric GCC-bOBP stabilized by the engineered disulfide bond is noticeably
348 shifted to higher denaturant concentrations. Curiously, the unfolding of complexes of all proteins
349 analyzed in this study with natural ligand OCT happens at the same denaturant concentrations.

350 Our data suggest that protein dimerization via the domain-swapping mechanism does not
351 contribute much to the increase in the conformational stability of a protein (at least in the case of
352 the analyzed in this study bOBP), despite the fact that the increased conformational stability was
353 proposed as one of the factors determining the use of this mechanism for dimer and higher
354 oligomer formation (Bennett et al. 1995; Liu & Eisenberg 2002). In contrast, introduction of a
355 disulfide bond to the structure of a monomeric protein shows significant stabilizing effects. Our
356 data also show that the formation of a protein-ligand complex leads to the significant
357 stabilization of different variants of bOBP and eliminates the original difference in
358 conformational stability caused by their structural differences.

359

ACKNOWLEDGEMENTS

This work was supported by a grant from the Russian Science Foundation RSCF № 14-24-00131.

AUTHOR CONTRIBUTIONS

Olga VS, Olesya VS and DOR collected and analyzed data, contributed to discussion, and wrote the manuscript. IMK and KKT conceived the idea, supervised the project, contributed to discussion, and reviewed/edited manuscript. VNU analyzed data, contributed to discussion, and wrote the manuscript.

DISCLOSURE

None declared.

REFERENCES

Bennett MJ, Schlunegger MP, and Eisenberg D. 1995. 3D domain swapping: a mechanism for oligomer assembly. *Protein Sci* 4:2455-2468.

Bianchet MA, Bains G, Pelosi P, Pevsner J, Snyder SH, Monaco HL, and Amzel LM. 1996. The three-dimensional structure of bovine odorant binding protein and its mechanism of odor recognition. *Nat Struct Biol* 3:934-939.

Bignetti E, Cavaggioni A, Pelosi P, Persaud KC, Sorbi RT, and Tirindelli R. 1985. Purification and characterisation of an odorant-binding protein from cow nasal tissue. *Eur J Biochem* 149:227-231.

Bignetti E, Damiani G, De Negri P, Romani R, Avanzini F, Ferrari G, and Rossi GL. 1987. Specificity of an immunoaffinity column for odorant-binding protein from bovine nasal mucosa. *Chem Senses* 12:601-608.

Boudjelal M, Sivaprasadarao A, and Findlay JB. 1996. Membrane receptor for odour-binding proteins. *Biochem J* 317 (Pt 1):23-27.

Briand L, Eloit C, Nespoulous C, Bezirard V, Huet JC, Henry C, Blon F, Trotier D, and Pernollet JC. 2002. Evidence of an odorant-binding protein in the human olfactory mucus: location, structural characterization, and odorant-binding properties. *Biochemistry* 41:7241-7252.

D'Auria S, Staiano M, Varriale A, Scognamiglio V, Rossi M, Parracino A, Campopiano S, Cennamo N, and Zeni L. 2006. The odorant-binding protein from Canis familiaris: purification, characterization and new perspectives in biohazard assessment. *Protein Pept Lett* 13:349-352.

Dal Monte M, Andreini I, Revoltella R, and Pelosi P. 1991. Purification and characterization of two odorant-binding proteins from nasal tissue of rabbit and pig. *Comp Biochem Physiol B* 99:445-451.

Dutta S, Burkhardt K, Young J, Swaminathan GJ, Matsuura T, Henrick K, Nakamura H, and Berman HM. 2009. Data deposition and annotation at the worldwide protein data bank. *Mol Biotechnol* 42:1-13.

Fan X, and Kurgan L. 2014. Accurate prediction of disorder in protein chains with a comprehensive and empirically designed consensus. *J Biomol Struct Dyn* 32:448-464.

Flower DR, North AC, and Sansom CE. 2000. The lipocalin protein family: structural and sequence overview. *Biochim Biophys Acta* 1482:9-24.

Grzyb J, Latowski D, and Strzalka K. 2006. Lipocalins - a family portrait. *J Plant Physiol* 163:895-915.

Hsin J, Arkhipov A, Yin Y, Stone JE, and Schulten K. 2008. Using VMD: an introductory tutorial. *Curr Protoc Bioinformatics* Chapter 5:Unit 5 7.

Ikematsu M, Takaoka D, and Yasuda M. 2005. Odorant binding initially occurring at the central pocket in bovine odorant-binding protein. *Biochem Biophys Res Commun* 333:1227-1233.

Jamroz M, Kolinski A, and Kihara D. 2012. Structural features that predict real-value fluctuations of globular proteins. *Proteins* 80:1425-1435.

Laemmli UK. 1970. Cleavage of structural proteins during the assembly of the head of bacteriophage T4. *Nature* 227:680-685.

Liu Y, and Eisenberg D. 2002. 3D domain swapping: as domains continue to swap. *Protein Sci* 11:1285-1299.

418 Mazzini A, Maia A, Parisi M, Sorbi RT, Ramoni R, Grolli S, and Favilla R. 2002. Reversible
419 unfolding of bovine odorant binding protein induced by guanidinium hydrochloride at
420 neutral pH. *Biochim Biophys Acta* 1599:90-101.
421 Merritt EA, and Bacon DJ. 1977. Raster3D: Photorealistic molecular graphics. . *Methods*
422 *enzymol* 277:505-524.
423 Pace CN. 1986. Determination and analysis of urea and guanidine hydrochloride denaturation
424 curves. *Methods Enzymol* 131:266-280.
425 Pelosi P, Baldaccini NE, and Pisanelli AM. 1982. Identification of a specific olfactory receptor
426 for 2-isobutyl-3-methoxypyrazine. *Biochem J* 201:245-248.
427 Peng K, Vucetic S, Radivojac P, Brown CJ, Dunker AK, and Obradovic Z. 2005. Optimizing
428 long intrinsic disorder predictors with protein evolutionary information. *J Bioinform*
429 *Comput Biol* 3:35-60.
430 Peng ZL, and Kurgan L. 2012. Comprehensive comparative assessment of in-silico predictors of
431 disordered regions. *Curr Protein Pept Sci* 13:6-18.
432 Pevsner J, and Snyder SH. 1990. Odorant-binding protein: odorant transport function in the
433 vertebrate nasal epithelium. *Chem Senses* 15:217-222.
434 Pevsner J, Trifiletti RR, Strittmatter SM, and Snyder SH. 1985. Isolation and characterization of
435 an olfactory receptor protein for odorant pyrazines. *Proc Natl Acad Sci U S A* 82:3050-
436 3054.
437 Ramoni R, Spinelli S, Grolli S, Conti V, Merli E, Cambillau C, and Tegoni M. 2008.
438 Deswapping bovine odorant binding protein. *Biochim Biophys Acta* 1784:651-657.
439 Ramoni R, Vincent F, Ashcroft AE, Accornero P, Grolli S, Valencia C, Tegoni M, and
440 Cambillau C. 2002. Control of domain swapping in bovine odorant-binding protein.
441 *Biochem J* 365:739-748.
442 Semisotnov GV, Rodionova NA, Razgulyaev OI, Uversky VN, Gripas AF, and Gilmanshin RI.
443 1991. Study of the "molten globule" intermediate state in protein folding by a
444 hydrophobic fluorescent probe. *Biopolymers* 31:119-128.
445 Shatsky M, Nussinov R, and Wolfson HJ. 2004. A method for simultaneous alignment of
446 multiple protein structures. *Proteins* 56:143-156.
447 Spinelli S, Ramoni R, Grolli S, Bonicel J, Cambillau C, and Tegoni M. 1998. The structure of
448 the monomeric porcine odorant binding protein sheds light on the domain swapping
449 mechanism. *Biochemistry* 37:7913-7918.
450 Staiano M, D'Auria S, Varriale A, Rossi M, Marabotti A, Fini C, Stepanenko OV, Kuznetsova
451 IM, and Turoverov KK. 2007. Stability and dynamics of the porcine odorant-binding
452 protein. *Biochemistry* 46:11120-11127.
453 Stepanenko OV, Bublikov GS, Stepanenko OV, Shcherbakova DM, Verkhusha VV, Turoverov
454 KK, and Kuznetsova IM. 2014a. A knot in the protein structure - probing the near-
455 infrared fluorescent protein iRFP designed from a bacterial phytochrome. *Febs J*
456 281:2284-2298.
457 Stepanenko OV, Fonin AV, Stepanenko OV, Morozova KS, Verkhusha VV, Kuznetsova IM,
458 Turoverov KK, Staiano M, and D'Auria S. 2011a. New insight in protein-ligand
459 interactions. 2. Stability and properties of two mutant forms of the D-galactose/D-
460 glucose-binding protein from E. coli. *J Phys Chem B* 115:9022-9032.
461 Stepanenko OV, Fonin AV, Stepanenko OV, Staiano M, D'Auria S, Kuznetsova IM, and
462 Turoverov KK. 2015. Tryptophan residue of the D-galactose/D-glucose-binding protein

from E. Coli localized in its active center does not contribute to the change in intrinsic fluorescence upon glucose binding. *J Fluoresc* 25:87-94.

Stepanenko OV, Marabotti A, Kuznetsova IM, Turoverov KK, Fini C, Varriale A, Staiano M, Rossi M, and D'Auria S. 2008. Hydrophobic interactions and ionic networks play an important role in thermal stability and denaturation mechanism of the porcine odorant-binding protein. *Proteins* 71:35-44.

Stepanenko OV, Povarova OI, Stepanenko OV, Fonin AV, Kuznetsova IM, Turoverov KK, Staiano M, and D'Auria S. 2009. Structure and stability of D-galactose/D-glucose-binding protein. The role of D-glucose binding and Ca ion depletion. *Spectrosc Biomed Appl* 24 355-359.

Stepanenko OV, Stepanenko OV, Kuznetsova IM, Shcherbakova DM, Verkhusha VV, and Turoverov KK. 2012. Distinct effects of guanidine thiocyanate on the structure of superfolder GFP. *PLoS One* 7:e48809.

Stepanenko OV, Stepanenko OV, Kuznetsova IM, Verkhusha VV, and Turoverov KK. 2013. Beta-barrel scaffold of fluorescent proteins: folding, stability and role in chromophore formation. *Int Rev Cell Mol Biol* 302:221-278.

Stepanenko OV, Stepanenko OV, Kuznetsova IM, Verkhusha VV, and Turoverov KK. 2014b. Sensitivity of superfolder GFP to ionic agents. *PLoS One* 9:e110750.

Stepanenko OV, Stepanenko OV, Povarova OI, Fonin AV, Kuznetsova IM, Turoverov KK, Staiano M, Varriale A, and D'Auria S. 2011b. New insight into protein-ligand interactions. The case of the D-galactose/D-glucose-binding protein from Escherichia coli. *J Phys Chem B* 115:2765-2773.

Stepanenko OV, Stepanenko OV, Staiano M, Kuznetsova IM, Turoverov KK, and D'Auria S. 2014c. The quaternary structure of the recombinant bovine odorant-binding protein is modulated by chemical denaturants. *PLoS One* 9:e85169.

Stephanenko OV, Roginskii DO, Stephanenko OV, Kuznetsova IM, Uversky VN, and Turoverov KK. 2015. Structure and stability of recombinant bovine odorant-binding protein: I. Design and analysis of monomeric mutants. . *PeerJ*.

Stryer L. 1965. The interaction of a naphthalene dye with apomyoglobin and apohemoglobin. A fluorescent probe of non-polar binding sites. *J Mol Biol* 13:482-495.

Tegoni M, Ramoni R, Bignetti E, Spinelli S, and Cambillau C. 1996. Domain swapping creates a third putative combining site in bovine odorant binding protein dimer. *Nat Struct Biol* 3:863-867.

Turoverov KK, Biktashev AG, Dorofeiuk AV, and Kuznetsova IM. 1998. [A complex of apparatus and programs for the measurement of spectral, polarization and kinetic characteristics of fluorescence in solution]. *Tsitologiia* 40:806-817.

Turoverov KK, and Kuznetsova IM. 2003. Intrinsic fluorescence of actin. *J Fluorescence* 13:41-57.

Vincent F, Spinelli S, Ramoni R, Grolli S, Pelosi P, Cambillau C, and Tegoni M. 2000. Complexes of porcine odorant binding protein with odorant molecules belonging to different chemical classes. *J Mol Biol* 300:127-139.

Xu P, Atkinson R, Jones DN, and Smith DP. 2005. Drosophila OBP LUSH is required for activity of pheromone-sensitive neurons. *Neuron* 45:193-200.

FIGURE LEGENDS

Figure 1. Analysis of the 3D structure of bOBP. Crystal 3D structures of natural bOBP (***A***) and monomeric mutant form GCC-bOBP (***B***). The individual subunits in the bOBP are in gray and orange. In the GCC-bOBP short α-helical segment that followed by the 9th β-strand and the disordered C-terminal region of the protein are drown in orange. The tryptophan residues are indicated in red and blue in the different subunits of bOBP and in blue in GCC-bOBP. The Gly 121+ residue which donates the increased mobility of the loop connecting α-helix and 8th β-strand of the β-barrel and promotes the formation of a monomeric fold of the mutant protein bOBP-Gly121+ is in green. Two cysteines residues Cys 64 and Cys 156 in GCC-bOBP, which are believed to stabilize monomeric structure due to the disulfide bond formation are in yellow. The drawing of bOBP and GCC-bOBP was generated based on the 1OBP (Tegoni et al. 1996) and 2HLV files (Ramoni et al. 2008) from PDB (Dutta et al. 2009) using the graphic software VMD (Hsin et al. 2008) and Raster3D (Merritt & Bacon 1977). Plot ***C*** represents the results of the multiple structural alignment of bOBP (PDB ID: 1OBP, blue structure), GCC-bOBP (PDB ID: 2HLV, red structure), and naturally monomeric pOBP (PDB ID: 1A3Y, green structure) using the MultiProt algorithm (http://bioinfo3d.cs.tau.ac.il/MultiProt/) (Shatsky et al. 2004). The drawing was generated using the graphic software VMD (Hsin et al. 2008). Plot ***D*** compares flexibility profiles obtained from crystal structures of bOBP (PDB ID: 1OBP, black and red lines for the chains A and B), naturally monomeric pOBP (PDB ID: 1A3Y, green and yellow lines for the chains A and B) and monomeric mutant GCC-bOBP (PDB ID: 2HLV, blue line) with the intrinsic disorder propensity of the bOBP (UniProt ID: P07435, pink dashed line). Flexibility profiles were obtained using the FlexPred software available at http://kiharalab.org/flexPred/ (Jamroz et al. 2012), whereas intrinsic disorder propensity was evaluated using the PONDR® VSL2 algorithm (Peng et al. 2005).

Figure 2. bOBP conformational changes induced by GdnHCl (the data are from (Stepanenko et al. 2014c)). ***A***: changes in fluorescence intensity at 320 nm, λ_{ex}=297 nm; ***B***: changes in parameter *A*, λ_{ex}=297 nm; ***C***: changes in fluorescence anisotropy at the emission wavelength 365 nm, λ_{ex}=297 nm; ***D***: changes in the ellipticity at 222 nm. The measurements were preceded by incubating the protein in a solution with the appropriate GdnHCl concentration at 4 ºC for 24 h. The open symbols indicate unfolding, whereas the closed symbols represent refolding. Changes in bOBP hydrodynamic dimensions for the different structural states were followed by the changes in the elution profiles for bOBP after pre-incubation for 24 h (solid lines) and 43 h (dashed line) with GdnHCl at the concentrations 0.0 (***E***), 0.5 (***F***) and 1.5 (***G***) for the denaturation process.

Figure 3. The changes of hydrodynamic dimensions of recombinant bOBP (*A* and *B*) and its complex with ligand bOBP/OCT (*C* and *D*) in different structural states. The elution profiles for bOBP and bOBP/OCT were recorded during the protein denaturation (***A*** and ***C***) and renaturation from unfolded states (***B*** and ***D***) induced by GdnHCl. The elution profiles for bOBP were measured after pre-incubation of the protein and the solution of GdnHCl in desired concentration for 24h (***A*** and ***B***), while in the case of bOBP/OCT the incubation time was extended to 72 – 84 h for denaturation (***C***) and 6 days for renaturation (***D***). The figures on the curves are the GdnHCl concentrations.

Figure 4. bOBP and bOBP/OCT conformational changes induced by GdnHCl. ***A***: changes in fluorescence intensity at 320 nm, λ_{ex}=297 nm; ***B***: changes in parameter *A*, λ_{ex}=297 nm; ***C***: changes in fluorescence anisotropy at the emission wavelength 365 nm, λ_{ex}=297 nm; ***D***: changes in the ellipticity at 222 nm; ***E***: changes in the ANS fluorescence intensity at λ_{ex}=365 nm, λ_{em}=480 nm.
The measurements were preceded by incubating the protein in a solution with the appropriate GdnHCl concentration at 4 ºC for 24 (red circles) in the case of bOBP. The open symbols indicate unfolding, whereas the closed symbols represent refolding.
While studying the folding of bOBP/OCT (squares), the solution of complex of the protein with its ligand were incubated in a solution with the appropriate GdnHCl concentration at 4 ºC for less than 24 h (open brown squares), up to 120 h (open pink squares) at the protein denaturation, and 1 h (closed brown squares) and 72 h – 30 days (closed pink squares) at the protein renaturation.

Figure 5. The changes of hydrodynamic dimensions of recombinant bOBP-Gly121+ (*A* and *B*) and its complex with ligand bOBP-Gly121+/OCT (*C* and *D*) in different structural states. The elution profiles for bOBP-Gly121+ and bOBP-Gly121+/OCT were recorded during the protein denaturation (***A*** and ***C***) and renaturation from unfolded states (***B*** and ***D***) induced by GdnHCl. The elution profiles for bOBP-Gly121+ were measured after pre-incubation of the protein and the solution of GdnHCl in desired concentration for 24h (***A*** and ***B***), while in the case of bOBP-Gly121+/OCT the incubation time was extended to 72 – 84 h for denaturation (***C***) and 6 days for renaturation (***D***). The figures on the curves are the GdnHCl concentrations.

Figure 6. Figure 4. bOBP-Gly121+ and bOBP-Gly121+/OCT conformational changes induced by GdnHCl. ***A***: changes in fluorescence intensity at 320 nm, λ_{ex}=297 nm; ***B***: changes in parameter *A*, λ_{ex}=297 nm; ***C***: changes in fluorescence anisotropy at the emission wavelength 365 nm, λ_{ex}=297 nm; ***D***: changes in the ellipticity at 222 nm; ***E***: changes in the ANS fluorescence intensity at λ_{ex}=365 nm, λ_{em}=480 nm.
The measurements were preceded by incubating the protein in a solution with the appropriate GdnHCl concentration at 4 ºC for 24 (dark green circles) in the case of bOBP-Gly121+. The open symbols indicate unfolding, whereas the closed symbols represent refolding.
While studying the folding of bOBP-Gly121+/OCT (squares), the solution of complex of the protein with its ligand were incubated in a solution with the appropriate GdnHCl concentration at 4 ºC for less than 24 h (open dark yellow squares), up to 72 h (open light green squares) at the protein denaturation, and 1 h (closed dark yellow squares) and 72 h (closed light green squares) at the protein renaturation.

Figure 7. The changes of hydrodynamic dimensions of recombinant GCC-bOBP (*A* and *B*) and its complex with ligand GCC-bOBP/OCT (*C* and *D*) in different structural states. The elution profiles for GCC-bOBP and GCC-bOBP/OCT were recorded during the protein denaturation (***A*** and ***C***) and renaturation from unfolded states (***B*** and ***D***) induced by GdnHCl. The elution profiles for GCC-bOBP were measured after pre-incubation of the protein and the solution of GdnHCl in desired concentration for 24h (***A*** and ***B***), while in the case of GCC-bOBP/OCT the incubation time was extended to 72 – 84 h for denaturation (***C***) and 6 days for renaturation (***D***). The figures on the curves are the GdnHCl concentrations.

598
599 **Figure 8. GCC-bOBP and GCC-bOBP/OCT conformational changes induced by GdnHCl.**
600 ***A***: changes in fluorescence intensity at 320 nm, λ_{ex}=297 nm; ***B***: changes in parameter *A*, λ_{ex}=297
601 nm; ***C***: changes in fluorescence anisotropy at the emission wavelength 365 nm, λ_{ex}=297 nm; ***D***:
602 changes in the ellipticity at 222 nm; ***E***: changes in the ANS fluorescence intensity at λ_{ex}=365 nm,
603 λ_{em}=480 nm.
604 The measurements were preceded by incubating the protein in a solution with the appropriate
605 GdnHCl concentration at 4 ºC for 24 (blue circles) in the case of GCC-bOBP. The open symbols
606 indicate unfolding, whereas the closed symbols represent refolding.
607 While studying the folding of GCC-bOBP/OCT (squares), the solution of complex of the protein
608 with its ligand were incubated in a solution with the appropriate GdnHCl concentration at 4 ºC
609 for less than 24 h (open dark blue squares), up to 72 h (open light blue squares) at the protein
610 denaturation, and 1 h (closed dark blue squares) and 72 h (closed light blue squares) at the
611 protein renaturation.
612
613 **Figure 9. Conformational changes of bOBP (red circles), bOBP-Gly121+ (green circles)**
614 **and GCC-bOBP (blue circles) and their complexes bOBP/OCT (pink squares), bOBP-**
615 **Gly121+/OCT (light green squares) and GCC-bOBP (light blue squares) induced by**
616 **GdnHCl.** ***A***: changes in fluorescence intensity at 320 nm, λ_{ex}=297 nm; ***B***: changes in parameter
617 *A*, λ_{ex}=297 nm; ***C***: changes in fluorescence anisotropy at the emission wavelength 365 nm,
618 λ_{ex}=297 nm; ***D***: changes in the ellipticity at 222 nm.
619 The equilibrium data for all studied proteins are compared. The open symbols indicate unfolding,
620 whereas the closed symbols represent refolding.

Table 1(on next page)

These are tables 1 and 2

Table 1. Characteristics of intrinsic fluorescence of recombinant bOBP in different structural states

Parameter	bOBP in buffered solution	bOBP in state I_1 (0.5 M GdnHCl)	bOBP in state I_2 (1.6 M GdnHCl)
λ_{max}, nm (λ_{ex}=297 nm)	335	337	335
Parameter *A* (λ_{ex}=297 nm)	1.2	1.1	1.2
r (λ_{ex}=297 nm, λ_{em}=365 nm)	0.170	0.166	0.180
τ, nm (λ_{ex}=297 nm, λ_{em}=335 nm)	4.4± 0.2	4.6±0.2	4.8±0.1

The data are from (Stepanenko et al. 2014c).

Table 2. Hydrodynamic dimensions of recombinant bOBPwt and its mutant forms in the absence and in the presence of natural ligand OCT in different structural states.

	GdnHCl, M	1 peak, kDa	2 peak, kDa
bOBPwt	0,0 0.5 1.5	43.9 34.0 43.6	23.8 19.3
bOBPwt/OCT	0.0 0.55 1.7	39.6 27.2 39.6	21.5 17.0
bOBP/Gly121+	0.0 0.25 1.5 – 1.9	23.6 17.8 24.8 – 28.5	
bOBP/Gly121+/OCT	0.0 0.24 – 0.5 1,7 – 2.0	21.5 15.5 – 16.2 24.7 – 28.5	
GCC-bOBP	0.0 0.25 1.1 – 1.82	23.6 17.8 22.5 – 25.9	
GCC-bOBP/OCT	0.0 0.27 1.5 – 2.0	22.5 16.9 22.5 – 27.2	

1

Analysis of the 3D structure of bOBP.

Crystal 3D structures of natural bOBP (***A***) and monomeric mutant form GCC-bOBP (***B***). The individual subunits in the bOBP are in gray and orange. In the GCC-bOBP short α-helical segment that followed by the 9th β-strand and the disordered C-terminal region of the protein are drown in orange. The tryptophan residues are indicated in red and blue in the different subunits of bOBP and in blue in GCC-bOBP. The Gly 121+ residue which donates the increased mobility of the loop connecting α-helix and 8th β-strand of the β-barrel and promotes the formation of a monomeric fold of the mutant protein bOBP-Gly121+ is in green. Two cysteines residues Cys 64 and Cys 156 in GCC-bOBP, which are believed to stabilize monomeric structure due to the disulfide bond formation are in yellow. The drawing of bOBP and GCC-bOBP was generated based on the 1OBP (Tegoni et al. 1996) and 2HLV files (Ramoni et al. 2008) from PDB (Dutta et al. 2009) using the graphic software VMD (Hsin et al. 2008) and Raster3D (Merritt & Bacon 1977). Plot ***C*** represents the results of the multiple structural alignment of bOBP (PDB ID: 1OBP, blue structure), GCC-bOBP (PDB ID: 2HLV, red structure), and naturally monomeric pOBP (PDB ID: 1A3Y, green structure) using the MultiProt algorithm (http://bioinfo3d.cs.tau.ac.il/MultiProt/) (Shatsky et al. 2004). The drawing was generated using the graphic software VMD (Hsin et al. 2008). Plot ***D*** compares flexibility profiles obtained from crystal structures of bOBP (PDB ID: 1OBP, black and red lines for the chains A and B), naturally monomeric pOBP (PDB ID: 1A3Y, green and yellow lines for the chains A and B) and monomeric mutant GCC-bOBP (PDB ID: 2HLV, blue line) with the intrinsic disorder propensity of the bOBP (UniProt ID: P07435, pink dashed line). Flexibility profiles were obtained using the FlexPred software available at http://kiharalab.org/flexPred/ (Jamroz et al. 2012), whereas intrinsic disorder propensity was evaluated using the PONDR® VSL2 algorithm (Peng et al. 2005).

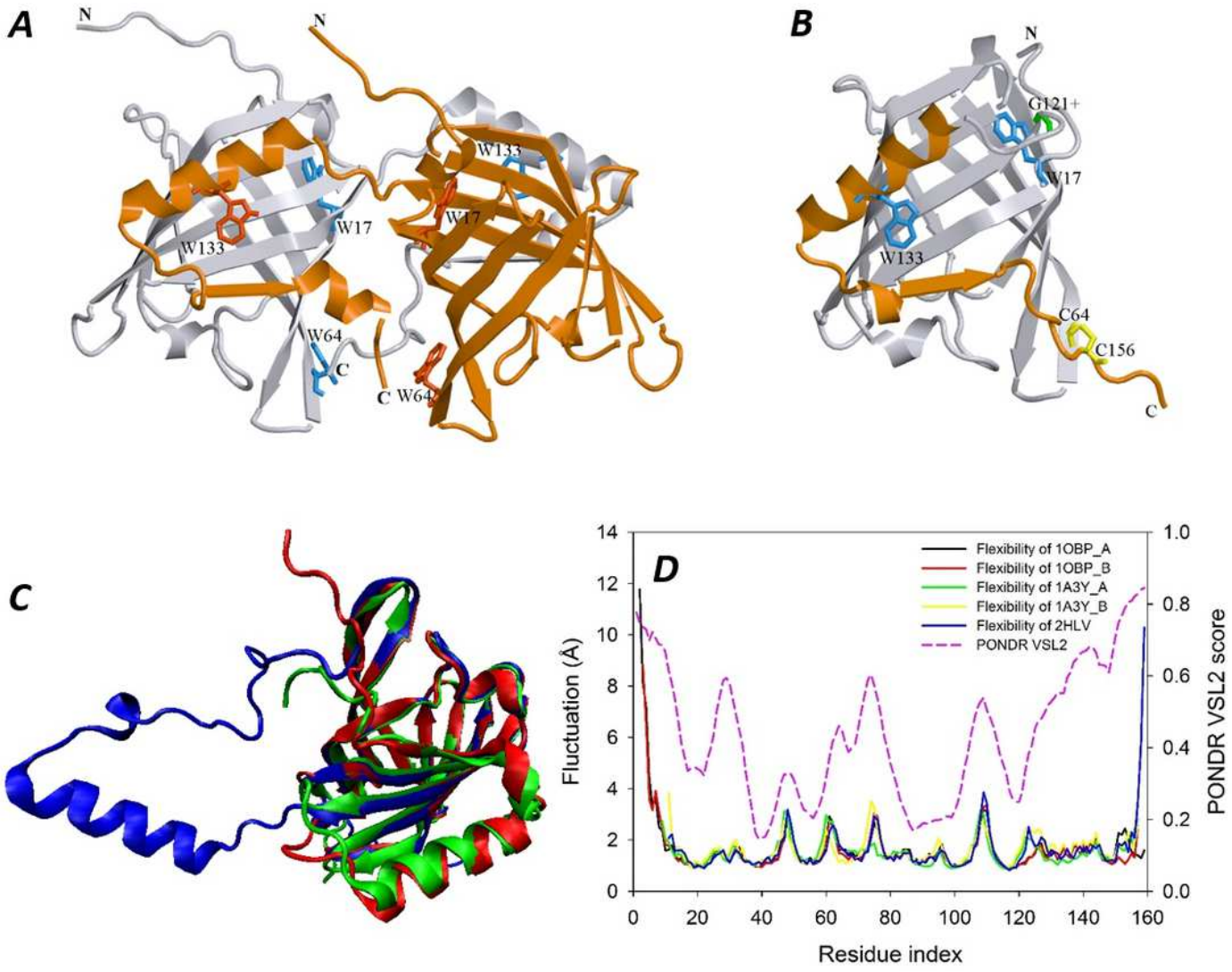

2

bOBP conformational changes induced by GdnHCl (the data are from (Stepanenko et al. 2014c)).

A: changes in fluorescence intensity at 320 nm, λ_{ex}=297 nm; ***B***: changes in parameter *A*, λ_{ex}=297 nm; ***C***: changes in fluorescence anisotropy at the emission wavelength 365 nm, λ_{ex}=297 nm; ***D***: changes in the ellipticity at 222 nm. The measurements were preceded by incubating the protein in a solution with the appropriate GdnHCl concentration at 4 ºC for 24 h. The open symbols indicate unfolding, whereas the closed symbols represent refolding. Changes in bOBP hydrodynamic dimensions for the different structural states were followed by the changes in the elution profiles for bOBP after pre-incubation for 24 h (solid lines) and 43 h (dashed line) with GdnHCl at the concentrations 0.0 (***E***), 0.5 (***F***) and 1.5 (***G***) for the denaturation process.

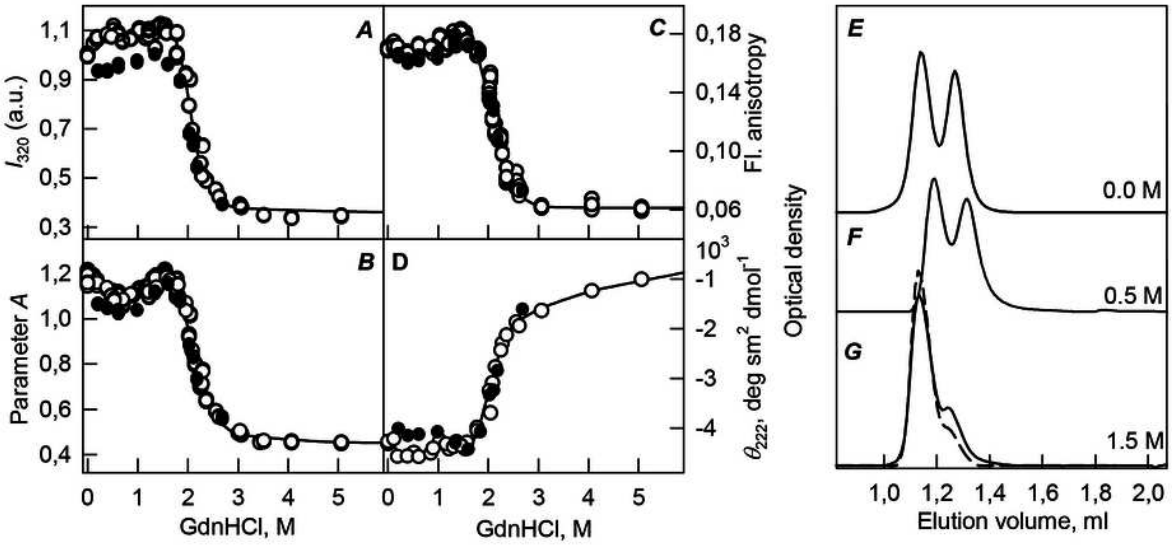

3

The changes of hydrodynamic dimensions of recombinant bOBP (*A* and *B*) and its complex with ligand bOBP/OCT (*C* and *D*) in different structural states.

The elution profiles for bOBP and bOBP/OCT were recorded during the protein denaturation (***A*** and ***C***) and renaturation from unfolded states (***B*** and ***D***) induced by GdnHCl. The elution profiles for bOBP were measured after pre-incubation of the protein and the solution of GdnHCl in desired concentration for 24h (***A*** and ***B***), while in the case of bOBP/OCT the incubation time was extended to 72 – 84 h for denaturation (***C***) and 6 days for renaturation (***D***). The figures on the curves are the GdnHCl concentrations.

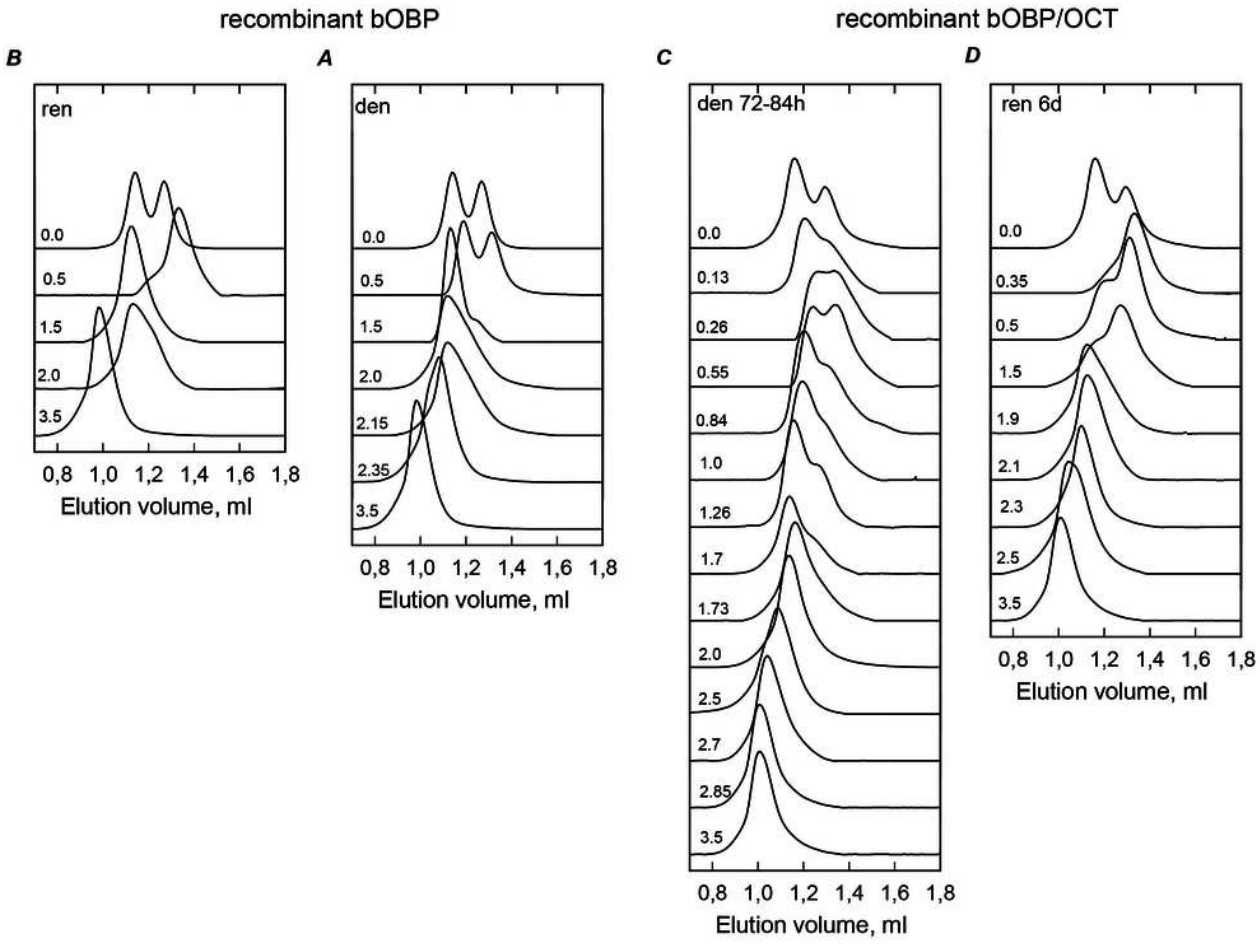

4

bOBP and bOBP/OCT conformational changes induced by GdnHCl.

A: changes in fluorescence intensity at 320 nm, λ_{ex}=297 nm; ***B***: changes in parameter *A*, λ_{ex}=297 nm; ***C***: changes in fluorescence anisotropy at the emission wavelength 365 nm, l_{ex}=297 nm; ***D***: changes in the ellipticity at 222 nm; ***E***: changes in the ANS fluorescence intensity at λ_{ex}=365 nm, λ_{em}=480 nm. The measurements were preceded by incubating the protein in a solution with the appropriate GdnHCl concentration at 4 ºC for 24 (red circles) in the case of bOBP. The open symbols indicate unfolding, whereas the closed symbols represent refolding. While studying the folding of bOBP/OCT (squares), the solution of complex of the protein with its ligand were incubated in a solution with the appropriate GdnHCl concentration at 4 ºC for less than 24 h (open brown squares), up to 120 h (open pink squares) at the protein denaturation, and 1 h (closed brown squares) and 72 h – 30 days (closed pink squares) at the protein renaturation.

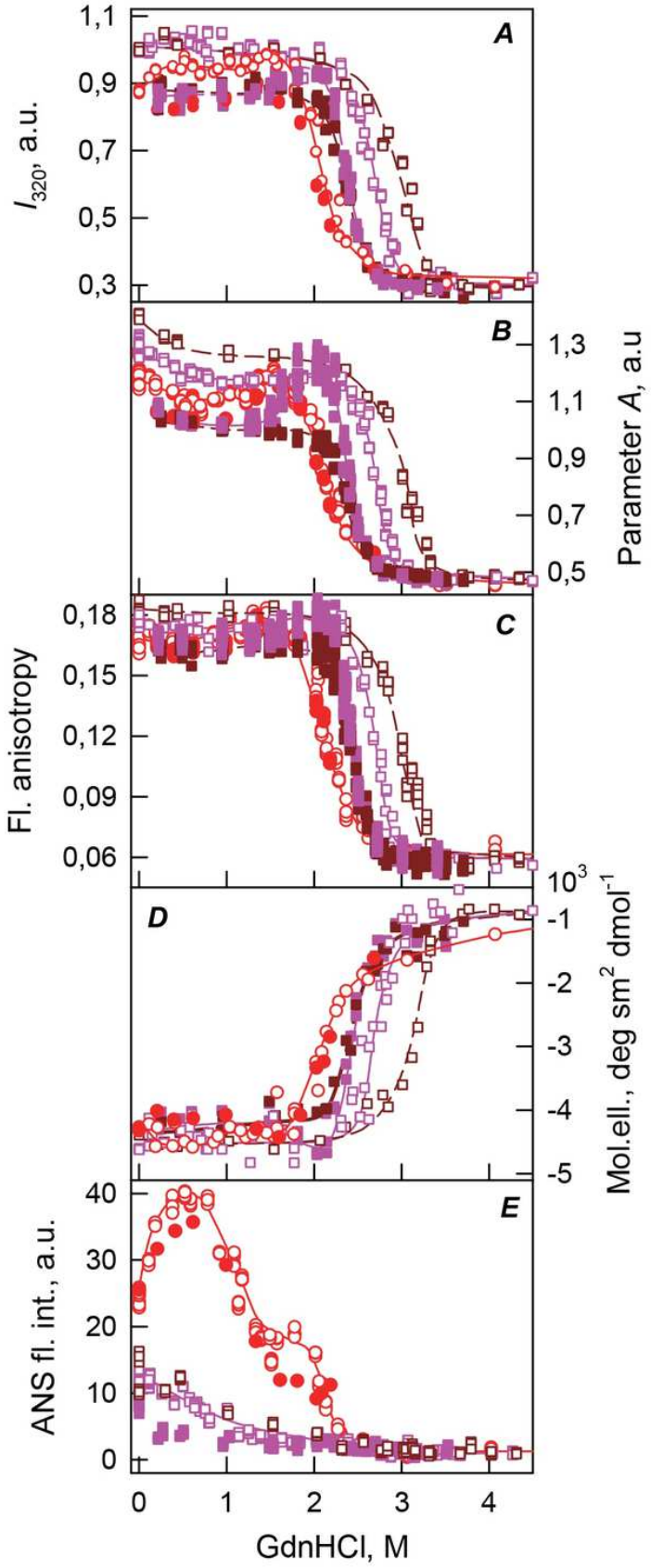

5

The changes of hydrodynamic dimensions of recombinant bOBP-Gly121+ (*A* and *B*) and its complex with ligand bOBP-Gly121+/OCT (*C* and *D*) in different structural states.

The elution profiles for bOBP-Gly121+ and bOBP-Gly121+/OCT were recorded during the protein denaturation (***A*** and ***C***) and renaturation from unfolded states (***B*** and ***D***) induced by GdnHCl. The elution profiles for bOBP-Gly121+ were measured after pre-incubation of the protein and the solution of GdnHCl in desired concentration for 24h (***A*** and ***B***), while in the case of bOBP-Gly121+/OCT the incubation time was extended to 72 – 84 h for denaturation (***C***) and 6 days for renaturation (***D***). The figures on the curves are the GdnHCl concentrations.

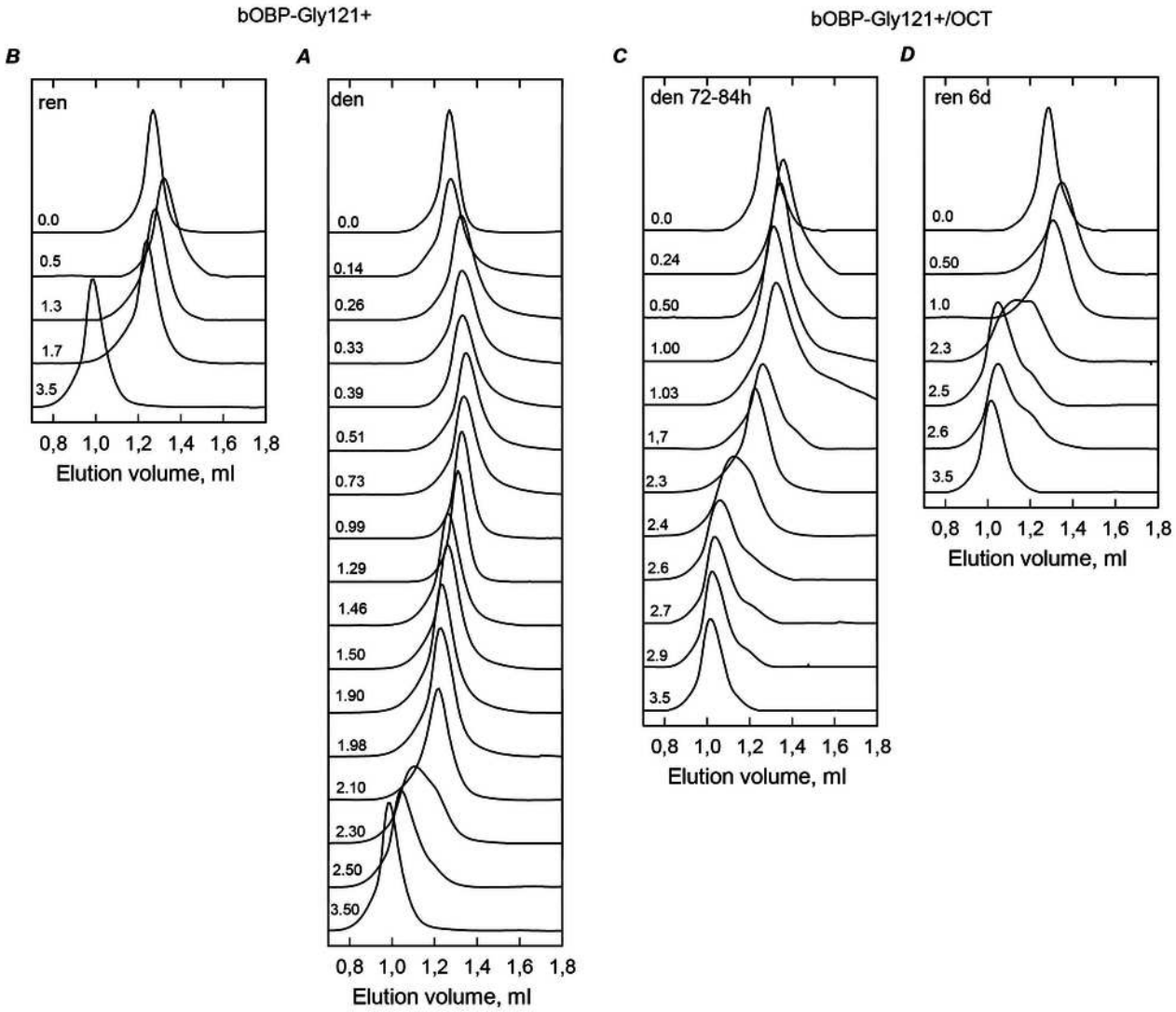

Figure 4. bOBP-Gly121+ and bOBP-Gly121+/OCT conformational changes induced by GdnHCl.

A: changes in fluorescence intensity at 320 nm, λ_{ex}=297 nm; ***B***: changes in parameter *A*, λ_{ex}=297 nm; ***C***: changes in fluorescence anisotropy at the emission wavelength 365 nm, l_{ex}=297 nm; ***D***: changes in the ellipticity at 222 nm; ***E***: changes in the ANS fluorescence intensity at λ_{ex}=365 nm, λ_{em}=480 nm. The measurements were preceded by incubating the protein in a solution with the appropriate GdnHCl concentration at 4 ºC for 24 (dark green circles) in the case of bOBP-Gly121+. The open symbols indicate unfolding, whereas the closed symbols represent refolding. While studying the folding of bOBP-Gly121+/OCT (squares), the solution of complex of the protein with its ligand were incubated in a solution with the appropriate GdnHCl concentration at 4 ºC for less than 24 h (open dark yellow squares), up to 72 h (open light green squares) at the protein denaturation, and 1 h (closed dark yellow squares) and 72 h (closed light green squares) at the protein renaturation.

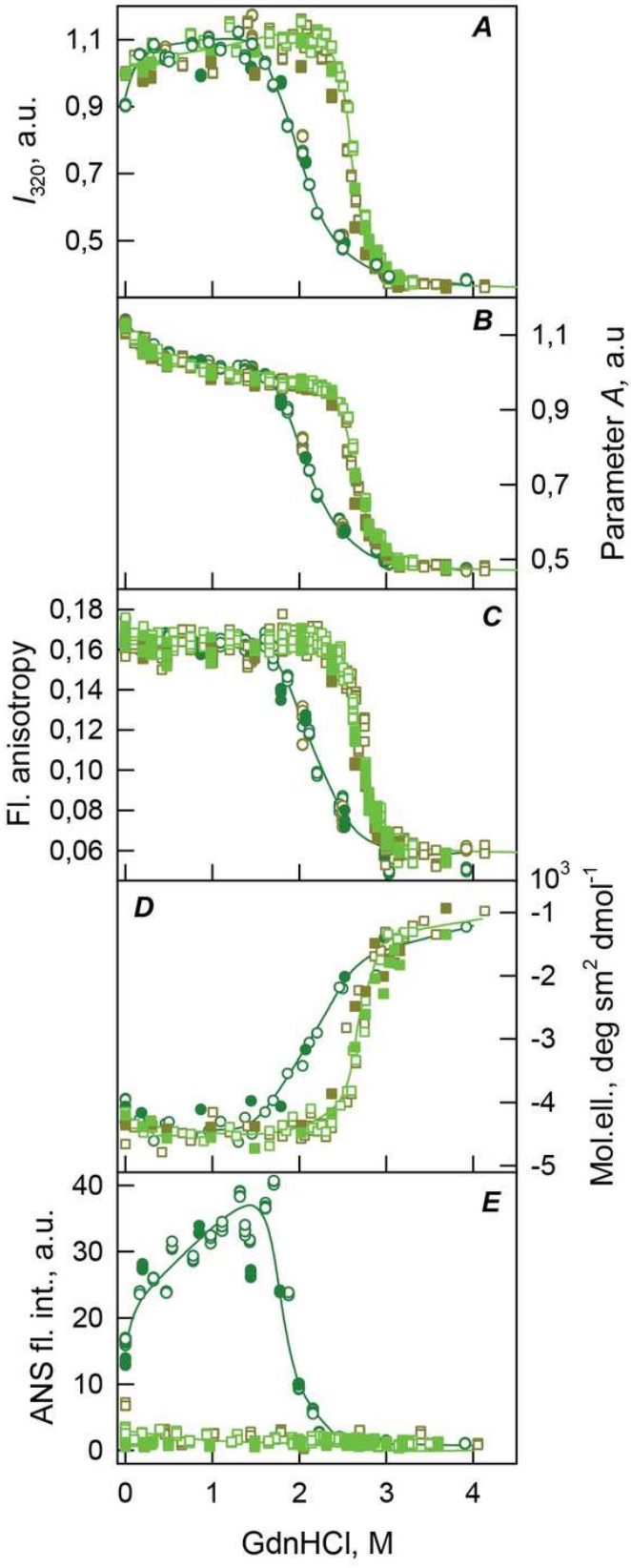

7

The changes of hydrodynamic dimensions of recombinant GCC-bOBP (*A* and *B*) and its complex with ligand GCC-bOBP/OCT (*C* and *D*) in different structural states.

The elution profiles for GCC-bOBP and GCC-bOBP/OCT were recorded during the protein denaturation (***A*** and ***C***) and renaturation from unfolded states (***B*** and ***D***) induced by GdnHCl. The elution profiles for GCC-bOBP were measured after pre-incubation of the protein and the solution of GdnHCl in desired concentration for 24h (***A*** and ***B***), while in the case of GCC-bOBP/OCT the incubation time was extended to 72 – 84 h for denaturation (***C***) and 6 days for renaturation (***D***). The figures on the curves are the GdnHCl concentrations.

PeerJ PrePrints | https://dx.doi.org/10.7287/peerj.preprints.1452v1 | CC-BY 4.0 Open Access | rec: 27 Oct 2015, publ: 27 Oct 2015

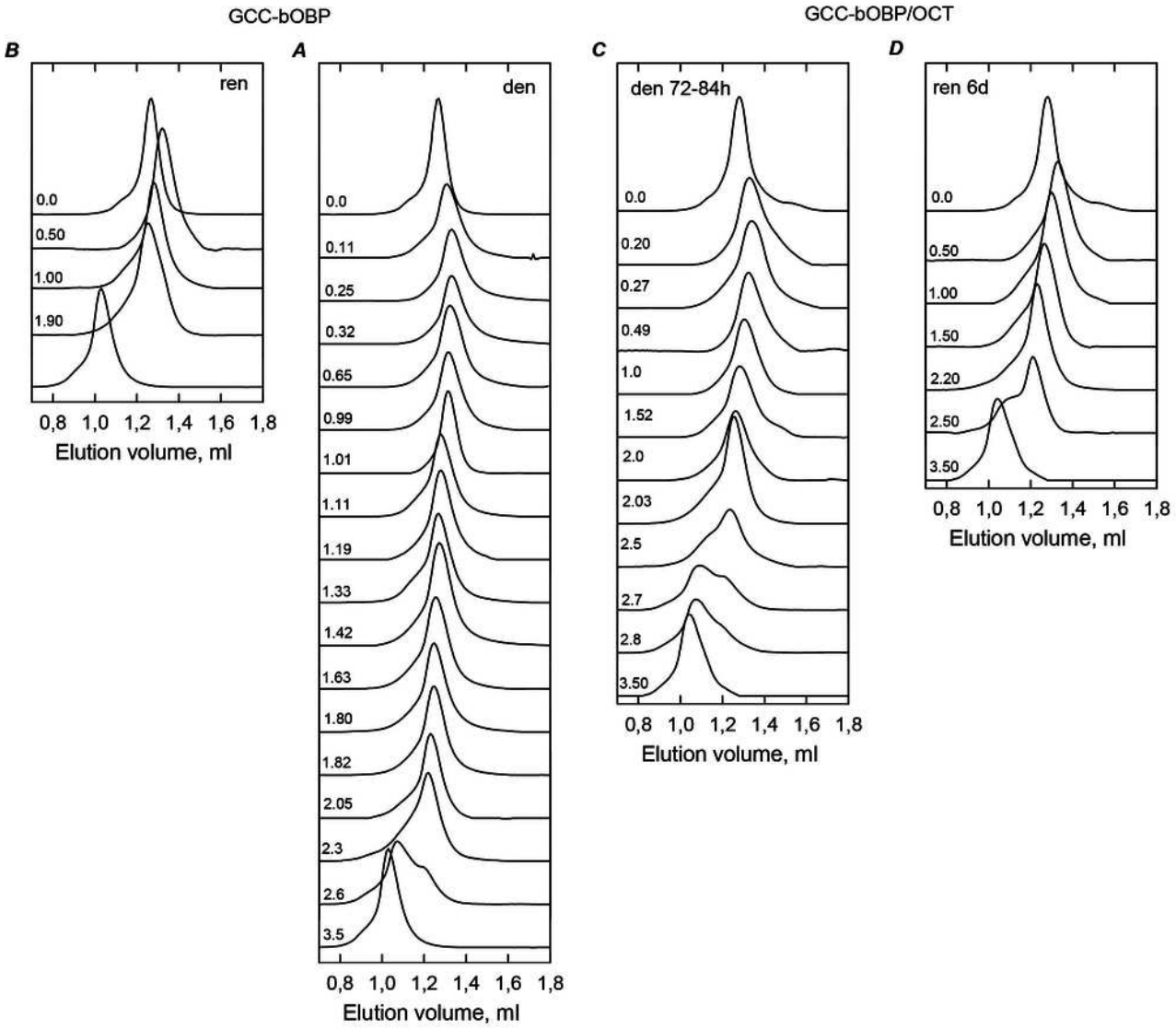

8

GCC-bOBP and GCC-bOBP/OCT conformational changes induced by GdnHCl.

A: changes in fluorescence intensity at 320 nm, λ_{ex}=297 nm; ***B***: changes in parameter *A*, λ_{ex}=297 nm; ***C***: changes in fluorescence anisotropy at the emission wavelength 365 nm, l_{ex}=297 nm; ***D***: changes in the ellipticity at 222 nm; ***E***: changes in the ANS fluorescence intensity at λ_{ex}=365 nm, λ_{em}=480 nm. The measurements were preceded by incubating the protein in a solution with the appropriate GdnHCl concentration at 4 ºC for 24 (blue circles) in the case of GCC-bOBP. The open symbols indicate unfolding, whereas the closed symbols represent refolding. While studying the folding of GCC-bOBP/OCT (squares), the solution of complex of the protein with its ligand were incubated in a solution with the appropriate GdnHCl concentration at 4 ºC for less than 24 h (open dark blue squares), up to 72 h (open light blue squares) at the protein denaturation, and 1 h (closed dark blue squares) and 72 h (closed light blue squares) at the protein renaturation.

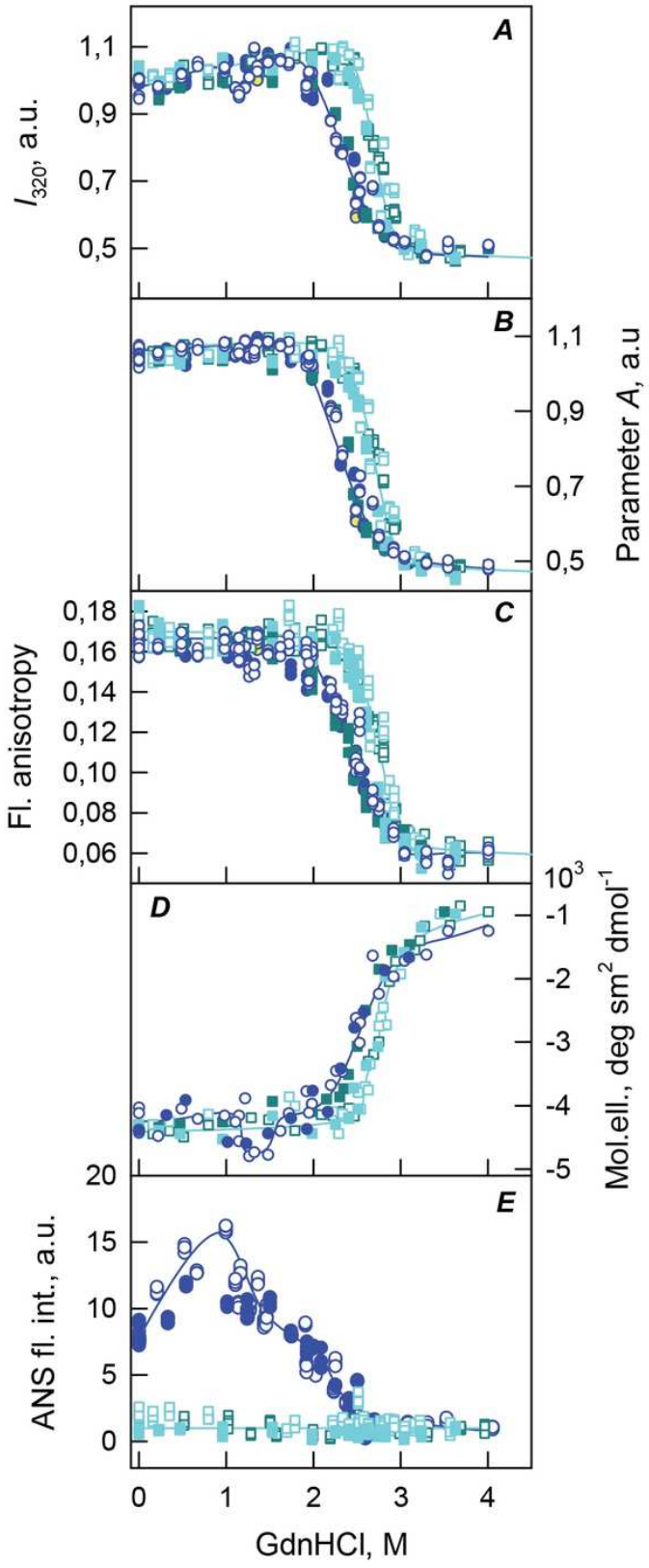

9

Figure 9. Conformational changes of bOBP (red circles), bOBP-Gly121+ (green circles) and GCC-bOBP (blue circles) and their complexes bOBP/OCT (pink squares), bOBP-Gly121+/OCT (light green squares) and GCC-bOBP (light blue squares) induced by GdnHCl.

A: changes in fluorescence intensity at 320 nm, λ_{ex}=297 nm; ***B***: changes in parameter *A*, λ_{ex}=297 nm; ***C***: changes in fluorescence anisotropy at the emission wavelength 365 nm, l_{ex}=297 nm; ***D***: changes in the ellipticity at 222 nm. The equilibrium data for all studied proteins are compared. The open symbols indicate unfolding, whereas the closed symbols represent refolding.